Excitation functions for $^{208-211}$Fr produced in the ^{18}O + ^{197}Au fusion reaction

L. Corradi, B. R. Behera, E. Fioretto, A. Gadea, A. Latina, A. M. Stefanini, S. Szilner,* M. Trotta, and Y. Wu
Istituto Nazionale di Fisica Nucleare, Laboratori Nazionali di Legnaro, Via Romea 4, I-35020 Legnaro, Padova, Italy

S. Beghini, G. Montagnoli, and F. Scarlassara
Dipartimento di Fisica, Universitá di Padova, and Istituto Nazionale di Fisica Nucleare, Sezione di Padova, Via Marzolo 8, I-35131 Padova, Italy

R. N. Sagaidak
Flerov Laboratory of Nuclear Reactions, Joint Institute for Nuclear Research, 141980, Dubna, Moscow Region, Russia

S. N. Atutov,† B. Mai, G. Stancari, and L. Tomassetti
Dipartimento di Fisica, Universitá di Ferrara, and Istituto Nazionale di Fisica Nucleare, Sezione di Ferrara, Via Paradiso 12, I-44100 Ferrara, Italy

E. Mariotti, A. Khanbekyan, and S. Veronesi
Dipartimento di Fisica, Universitá di Siena, and Istituto Nazionale di Fisica della Materia, Via Roma 56, I-53100 Siena, Italy
(Received 5 February 2004; published 27 January 2005)

Excitation functions for $^{208-211}$Fr isotopes produced in the ^{18}O + ^{197}Au fusion-evaporation reaction have been measured at $E_{lab} = 75$–130 MeV via characteristic α decays by means of an electrostatic deflector and a semiconductor detector. Data have been compared with calculations giving barrier-passing (capture) cross sections and probabilities of the compound nucleus decay into different channels according to the standard statistical model.

DOI: 10.1103/PhysRevC.71.014609 PACS number(s): 25.70.Gh, 25.70.Jj

I. INTRODUCTION

Reactions leading to Fr nuclei are excellent cases for studying fusion in the pre-actinide region, and knowledge of evaporation residue (ER) cross sections at energies close to the Coulomb barrier is interesting from various point of views. Francium is close to radium and recently fusion cross sections for Ra have been found [1,2] to be significantly reduced even in very asymmetric combinations. Since it is now clear that a description of fusion of massive nuclei must go beyond the conventional potential-barrier passing models applicable to medium-mass systems [3], further data in this region may help to better understand the interplay between compound nucleus (CN) formation and the onset of competing reaction channels [4–8]. Francium is located where octupole deformed nuclear states are predicted and cross-section measurements are very useful to properly fix spectroscopic measurements in searching for feeble electromagnetic transitions [9]. Francium nuclei are also presently considered key to electroweak interaction studies, since their atoms are the heaviest alkalines that can be produced (see [10,11] and references therein for an overview in this field). Fusion-evaporation reactions are very suitable for the production of $^{208-211}$Fr, whose characteristics (lifetimes, α-branching ratios, and atomic level schemes) make them optimal candidates for precision experiments with traps. These isotopes can be produced via ^{197}Au(^{18}O, xn)$^{215-x}$Fr reactions in the 100–120-MeV energy range [10,12]. Precise knowledge of absolute cross sections is important for setting experimental parameters to maximize the production yield of Fr [12].

We report here on measurements performed with the ^{18}O + ^{197}Au reaction to derive ER cross sections for specific Fr isotopes in an energy range from slightly below to about 40% above the Coulomb barrier. Data are compared with calculations giving the barrier-passing (capture) cross sections and probabilities of the CN decay into different channels according to the standard statistical model [13]. A comparison is also performed with data available for neighboring Fr compound nuclei formed in similar asymmetric projectile-target combinations.

II. THE EXPERIMENT AND RESULTS

The experiment was performed at the XTU-Tandem accelerator of the Laboratori Nazionali di Legnaro. An ^{18}O beam was delivered at bombarding energies in the range 75–130 MeV with an average intensity of 15 pnA onto a self-supporting 150-μg/cm^2 ^{197}Au target. Francium isotopes produced via neutron evaporation channels from the ^{215}Fr* CN were separated from beamlike particles by means of an electrostatic deflector [14] connected to a sliding-seal scattering chamber. Evaporation residues were directly implanted into a silicon surface-barrier detector (SSBD) placed behind

*Present address: Ruđer Bošković Institute, HR-10 002 Zagreb, Croatia.

†Permanent address: Institute of Automation and Electrometry, Novosibirsk 90, Russia.

TABLE I. α-decay properties of Fr isotopes [15] produced in the $^{18}O + ^{197}Au$ experiment.

Isotope	E_α (MeV)	α branch (%)	Half-life (s)
^{208}Fr	6.641	90	59.1
^{209}Fr	6.646	89	50.0
^{210}Fr	6.543	60	191
^{211}Fr	6.534	$\geqslant 80$	186

the deflector. Corresponding α decays of stopped ERs were detected. This allowed us to get absolute cross sections (σ) for specific Fr isotopes, eliminating possible bias in the ER data due to incomplete fusion events.

Four silicon detectors were installed inside the scattering chamber to measure Rutherford scattered beam particles for absolute normalization of cross sections and relative normalization among different runs. These detectors were also used to correct for changes of the beam position on the target.

Table I shows the main α-decay properties (α energy, α-branching ratio, and half-life) for the $^{208-211}$Fr isotopes [15] produced in our experiment. Figure 1 is an example of an α-energy spectrum obtained at $E_{\rm lab} = 97.5$ MeV with the electrostatic deflector placed at -2° to reduce the background of beamlike particles. The α energies within the ^{208,209}Fr and ^{210,211}Fr groups are not resolved because the SSBD resolution $\simeq$40 keV (FWHM). The third prominent peak ($E_\alpha \simeq 6.04$ MeV) corresponds to the ^{209,210}Rn nuclei produced via EC + β^+ decays of ^{209,210}Fr [15] and in the $p4n$ and $p5n$ evaporation channels of the ^{215}Fr* CN. Production of these nuclei were not considered within the time limitation of the present experiment because their lifetimes are much longer

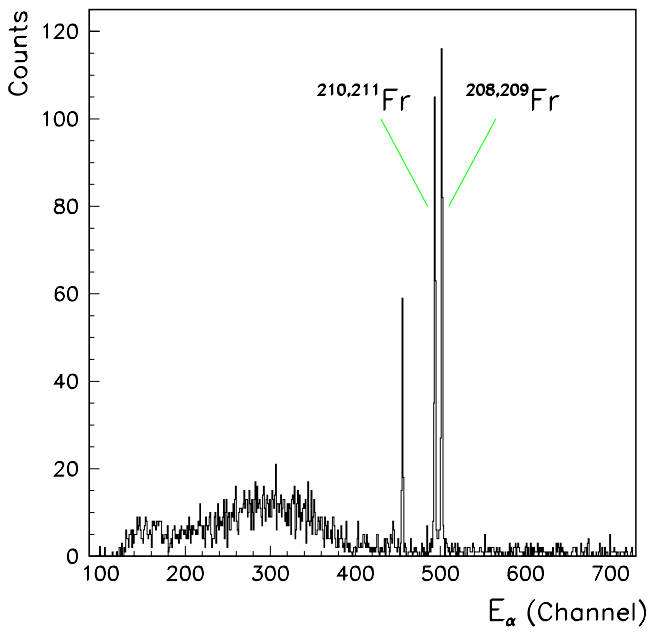

FIG. 1. (Color online) Energy spectrum obtained in $^{18}O + ^{197}Au$ at $E_{\rm lab} = 97.5$ MeV with the SSBD installed behind the electrostatic deflector (see text).

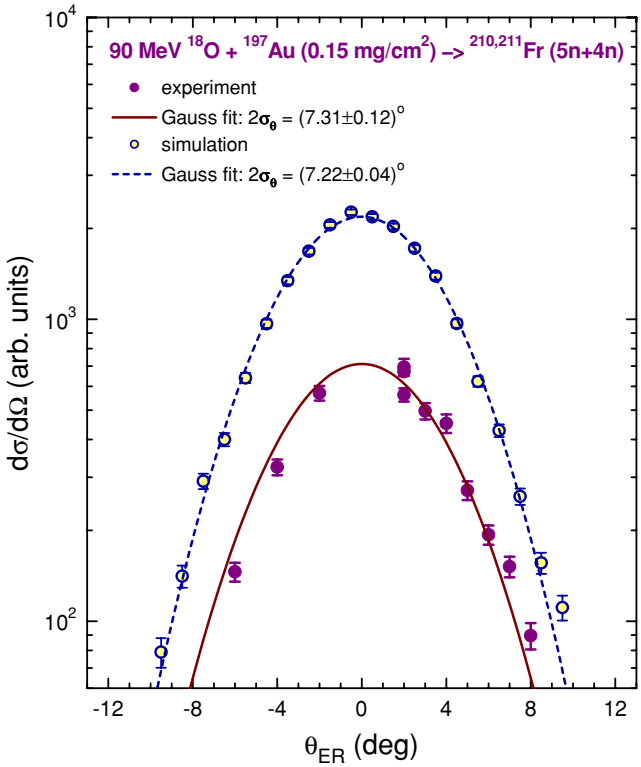

FIG. 2. (Color online) Experimental (filled circles) and simulated (open circles) angular distributions at $E_{\rm lab} = 90$ MeV. Widths ($2\sigma_\theta$) resulting from Gaussian fits (lines) are indicated.

than those for Fr isotopes. Calculations performed with the HIVAP code [13] (see Sec. III) show that $\sigma_{p4n+p5n} \lesssim \sigma_{5n+6n}$ at about the same excitation energy. The bump in the low-energy part of the spectrum in Fig. 1 corresponds to the ERs implanted into the SSBD.

The ratio of events collected in the α peaks and in the monitors, after proper normalization, allowed us to obtain differential cross sections for the ERs. Angular distributions were measured at $E_{\rm lab} = 90$ MeV in the angular range from -6° to $+8^\circ$ to get the integral cross section for the production of Fr isotopes. The data are shown in Fig. 2 for the ^{210,211}Fr group, together with simulations (to be discussed in the following). The width of the simulated distribution is very close to the experimental one. The former varies weakly with the bombarding energy, but the integral cross sections at higher and lower bombarding energies were corrected using the simulations since their values depend quadratically on the width itself. Maximal values of this correction correspond to $+14\%$ at the lowest energy and -10% at the highest one; these corrections were applied to the cross sections obtained from the experimental width at 90 MeV.

The transmission factor of the electrostatic deflector (relatively to the solid angle subtended by the SSBD) including the trajectory distortion caused by the electric field, energy and atomic charge state distributions for the ERs has been derived through a Monte Carlo simulation and compared with the measured yield of ^{210,211}Fr at 90 MeV as a function of the high voltage applied to the deflector. This yield is shown

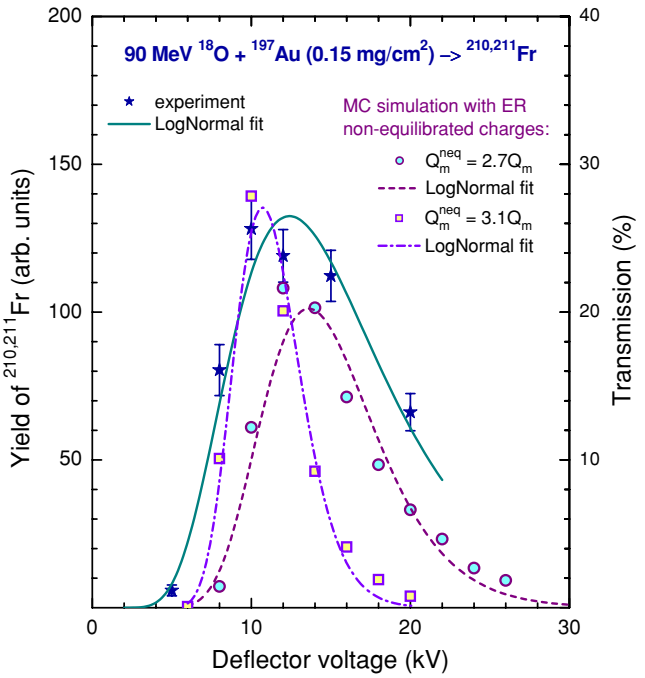

FIG. 3. (Color online) Comparison of the measured ^{210,211}Fr yield (stars) vs. high voltage with the simulations (circles and squares) for the nonequilibrated charge distribution parametrically scaled (Q_m^{neq} values are indicated in units of Q_m and $\Delta Q^{neq} = 3\Delta Q$) with respect to the equilibrated one [17]. One-component log-normal-function fits are shown by different lines. The right ordinate scale corresponds to the transmission of the deflector [14].

in Fig. 3. We assumed two components in the charge state distribution (i.e., an equilibrated and a nonequilibrated one), as was observed in similar measurements in ^{16}O + ^{197}Au [16]. The measured yield corresponds to the nonequilibrated component, in agreement with the data of Ref. [16]. This nonequilibrated component favoring higher atomic charge states likely comes from long-lived nuclear states decaying through Auger cascades after internal conversion. This component, in turn, consists of two components [16], which are poorly resolved in our measurements (a one-component fit to the data with a log-normal distribution function is shown in Fig. 3). These two nonequilibrated components can be reproduced in a simulation with a scaling of the parameter values describing the equilibrated charge distribution given by systematics for the mean charge Q_m and width ΔQ [17], as shown in Fig. 3.

From our fit of the ER yield obtained in ^{16}O + ^{197}Au [16] with the three-component (two nonequilibrated components and the equilibrated one) log-normal distribution function, we find that the nonequilibrated part corresponds to $\simeq$75% of the total. Our Monte Carlo simulation (similar to the one used earlier [2]) shows that from 20% to 26% of ERs having nonequilibrated charges can be delivered to the SSBD at the high voltage corresponding to the maximal yield (see Fig. 3). Uncertainties in the estimates of the ER transmission comprised the main contribution to overall errors in our final cross sections, which we quote to be within $\pm$20%.

TABLE II. Experimental total cross sections (σ) in millibarns for the different groups of Fr isotopes produced in the ^{18}O + ^{197}Au experiment. Errors are quoted to be $\pm$20%.

E_{lab}^{a} (MeV)	σ(^{210,211}Fr)	σ(^{208,209}Fr)	σ(^{207}Fr)
74.9	1.1		
79.9	54.0		
84.9	198.8		
87.4	206.2		
89.9	223.9		
89.9	218.3		
92.4	160.4		
94.9	115.1	23.9	
97.4	66.4	55.1	
99.9	36.3	73.3	
104.9	12.3	106.3	
109.9		96.1	
114.9		71.7	
119.9		41.2	5.3
124.9		24.5	16.0
129.9		10.4	19.9

[a] Corrected for stopping in a half-thickness of the target.

The experimental integral cross sections for the different Fr isotopes produced in the ^{18}O + ^{197}Au fusion reaction are reported in Table II. In Fig. 4 the data are shown together with calculations discussed in the next section. As the bombarding energy increases from below the nominal fusion barrier [18] (indicated by an arrow in Fig. 4) the total ER cross section first increases very rapidly, then reaches a maximum, and finally starts to decrease, owing to the onset of the various competing reaction channels (mainly fission, unmeasured in this experiment).

As already noted in Sec. I, Fr is presently considered as a key nucleus for fundamental interaction studies [10,11]. The $^{208-211}$Fr isotopes are produced at Stony Brook [10] and Legnaro [12] with an ^{18}O beam in the microampere range hitting a thick ^{197}Au target. At Legnaro, the products are extracted from a specially designed source and reaccelerated at a few thousand electron volts as a secondary radioactive beam to a laser area, where a magneto-optic trap has been recently installed (we refer to the cited references for the details). The beam energy is normally kept in the E_{lab} range of 100–105 MeV to maximize the production yield of ^{210}Fr, which is the easiest isotope to handle in the trap experiment. The rate at the target location involves three factors: fusion-evaporation cross sections, transport efficiency inside the bulk material, and release efficiency from the surface. The excitation functions measured in the present work will be important for making quantitative estimates of the factors that eventually limit the production yield.

III. DISCUSSION

The details on how the fusioning system evolves dynamically are presently not well understood. Passing the Coulomb barrier does not guarantee complete equilibration of all the

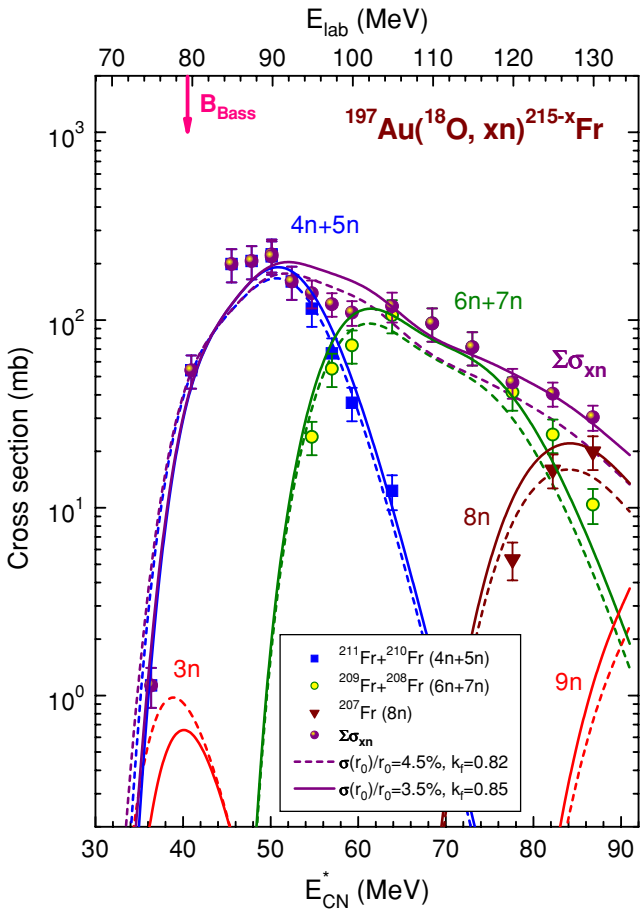

FIG. 4. (Color online) Measured excitation functions for the production of Fr isotopes in ^{197}Au(^{18}O, xn) reactions (symbols) compared with calculations (lines) performed with HIVAP [13].

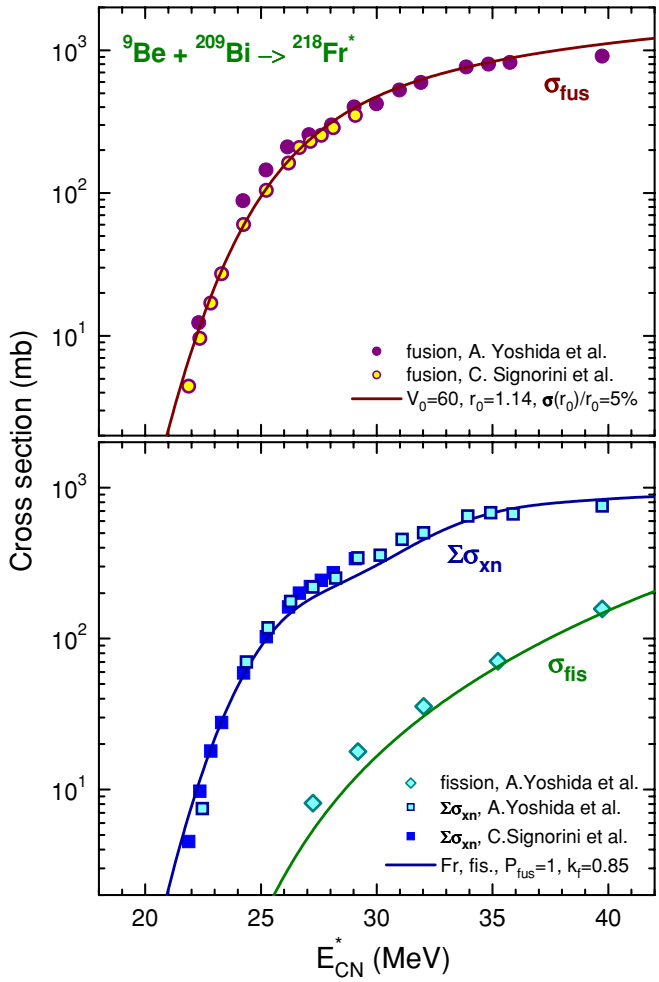

FIG. 5. (Color online) ^{9}Be + ^{209}Bi excitation functions for the fusion (upper panel) and fission and production of Fr nuclei (bottom panel) as obtained in [26,27] (symbols) compared with calculations (lines) performed with HIVAP [13].

degrees of freedom with a formation of a compact mononucleus and ensuing complete fusion. Competing processes, such as quasi-fission and deep-inelastic collisions, force the "dinuclear system" to reseparate after large energy losses take place [4–8]. Complete experimental information on these reaction channels would be needed to properly study to what extent CN formation becomes limited. In the present work, although the data set is restricted to ER only, we compared consistently our new and other experimental data with the same model calculations.

The calculations were performed within the framework of the barrier-passing model (BPM) and standard statistical model (SSM) incorporated into the HIVAP code [13]. In the BPM we used the exponential nuclear potential with the sharp radius correction and the same values of parameters (radius parameter $r_0 = 1.12$ fm, diffuseness $d = 0.75$ fm, and depth of the nuclear potential $V_0 = 75$ MeV/fm) used earlier [2] for the description of the ^{19}F + ^{197}Au ER and fission excitation functions [1]. The effect of coupling the entrance channel to other reaction channels is taken into account via fluctuations of r_0, which are generated with a Gaussian distribution around its average value, with the barrier fluctuation parameter $\sigma(r_0)$ [19]. These fluctuations, at energies around the Coulomb barrier, simulate coupling effects [20] to a degree sufficient for the purpose of the present analysis. In our case, $\sigma(r_0)/r_0$ is around 4%, a value that allows us to describe the ER and fission data corresponding to mass-asymmetric combinations with moderately deformed target nuclei [2].

For fissile compound nuclei, the ER cross sections at energies well above the Coulomb barrier are weakly sensitive to the form of the nuclear potential and are mainly determined by the SSM parameters describing the CN deexcitation. The important parameters are the level-density parameters in the fission and evaporation channels, $\tilde{a}_f$ and $\tilde{a}_\nu$, respectively, the scaling factor k_f at the rotating liquid-drop (LD) fission barriers [21] $B_f^{\mathrm{LD}}(l)$, and the ground-state shell correction ΔW_{gs} (the difference between the empirical and LD masses). The ratio of the level-density parameters $\tilde{a}_f/\tilde{a}_\nu$ slightly exceeds unity owing to the different nuclear shapes at the saddle point (fission) and equilibrium state (particle evaporation) [13]. Empirical masses [22] were used to calculate ΔW_{gs} as well as the excitation and separation energies.

At energies well above the fusion barrier, results of calculations depend essentially only on k_f, which reduces fission

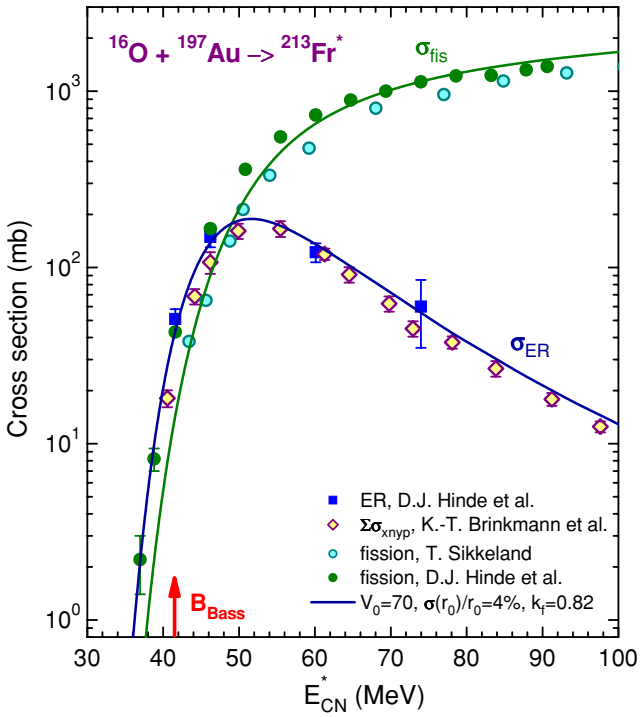

FIG. 6. (Color online) ^{16}O + ^{197}Au excitation functions for ER and fission as obtained in [16,28,29] (symbols) compared with calculations (lines) performed with HIVAP [13].

barriers $B_f(l)$ according to the scaling $B_f(l) = k_f B_f^{\mathrm{LD}}(l) - \Delta W_{\mathrm{gs}}$. With the values $k_f = 0.82$–0.85 and assuming unitary fusion probability $P_{\mathrm{fus}} = 1$ (i.e., all partial waves passing through the potential barrier lead to fusion), one could describe both ER and fission excitation functions for the ^{12}C + ^{204,206,208}Pb systems [2]. For the present system, assuming $P_{\mathrm{fus}} = 1$ and using $k_f = 0.85$, $V_0 = 75$ MeV/fm, and $\sigma(r_0)/r_0 = 3.5\%$, our calculations reproduce rather well the measured excitation functions for the Fr-isotope groups and for the summed cross-section $\Sigma\sigma_{xn}$, as shown in Fig. 4. To get a feeling for the sensitivity of the computed cross sections to k_f we also show the calculations using $k_f = 0.82$. Recall that a scaling of the LD barriers is commonly used in the analysis of the cross-section data for ERs produced in reactions leading to fissile compound nuclei (see, e.g., [23,24]) since our knowledge of the macroscopic deformation energy of nuclei is lacking. In our case, the 15% scaling leads to LD barrier values close to the ones obtained within the framework of the finite range model [25].

It is interesting to compare the quality of agreement between experimental and calculated cross sections for mass-asymmetric combinations leading to neighboring Fr compound nuclei. We performed this analysis with the available data corresponding to the formation of ^{213,217,218}Fr*. We show in the following two cases where both experimental ER and fusion-fission cross sections are available; this will allow us to put a tighter constraint on the choice of model parameter values.

The results for the most neutron-rich ^{218}Fr* CN produced in the very asymmetric ^{9}Be + ^{209}Bi [26,27] system are shown in Fig. 5. As we see, both ER and fission excitation functions are well described with $k_f = 0.85$, keeping the assumption of unitary fusion probability ($P_{\mathrm{fus}} = 1$). Figure 6 shows the results of our data analysis for the ER production and fission in ^{16}O + ^{197}Au leading to the neutron-deficient ^{213}Fr* CN [16,28,29]. The data are reproduced quite well with $k_f = 0.82$, by assuming that the experimental cross sections specified as σ_{xnyp} in Ref. [16] correspond to the ER cross sections obtained in the calculation. For the fission cross sections, the results of calculations lie between the data [28,29], which differ from each other to some extent. A quite satisfactory agreement is obtained for ER data corresponding to the production of Fr isotopes in specific xn evaporation channels [30] with $k_f = 0.85$. We see that the general agreement between experiments and calculations for the neighboring ^{16}O + ^{197}Au system is similar to our ^{18}O + ^{197}Au case.

IV. SUMMARY

Excitation functions for different groups of Fr isotopes produced in the ^{197}Au(^{18}O, xn) fusion-evaporation reactions have been measured at energies close to the Coulomb barrier. These excitation functions will be important for future studies of feeble electromagnetic transitions and for experiments with traps. The data can be reproduced in calculations using the barrier-passing model for CN formation and treating the CN decay according to the standard statistical model. The comparison with reactions leading to neighboring Fr compound nuclei produced in similar asymmetric projectile-target combinations shows the same quality of agreement.

It would be interesting to perform further measurements in this region [31], choosing systems leading to the same CN, but with different entrance-channel mass asymmetry. In particular, a detailed understanding of the mechanism of limitations observed in fusion [1] near the Businaro-Gallone point [32] for systems with similar entrance-channel mass asymmetry is desirable. Reactions leading to Fr nuclei (which are less fissile than Ra ones) are, in this respect, excellent cases for such studies in the pre-actinide CN region. In such reactions correlation of the fusion probability with the entrance-channel mass asymmetry and CN fissility seems to be quite evident [31].

[1] A. C. Berriman, D. J. Hinde, M. Dasgupta, C. R. Morton, R. D. Butt, and J. O. Newton, Nature **413**, 144 (2001); D. J. Hinde, A. C. Berriman, R. D. Butt, M. Dasgupta, I. I. Gontchar, C. R. Morton, A. Mukherjee, and J. O. Newton, J. Nucl. Radiochem. Sci. **3**, 31 (2002).

[2] R. N. Sagaidak *et al.*, Phys. Rev. C **68**, 014603 (2003).

[3] M. Dasgupta, D. J. Hinde, N. Rowley, and A. M. Stefanini, Annu. Rev. Nucl. Part. Sci. **48**, 401 (1998).
[4] J. Tōke *et al*., Nucl. Phys. **A440**, 327 (1985).
[5] W. O. Shen *et al*., Phys. Rev. C **36**, 115 (1987).
[6] W. Reisdorf, J. V. Kratz, R. Bellwied, W. Brüchle, H. Keller, K. Lützenkirchen, M. Schädel, K. Sümmerer, and G. Wirth, Z. Phys. A **342**, 411 (1992).
[7] P. Klein, J. V. Kratz, M. K. Gober, H. P. Zimmermann, W. Brüchle, W. Reisdorf, and M. Schädel, Z. Phys. A **357**, 193 (1997).
[8] D. J. Hinde, M. Dasgupta, and A. Mukherjee, Phys. Rev. Lett. **89**, 282701 (2002).
[9] J. F. C. Cocks *et al*., Nucl. Phys. **A645**, 61 (1999).
[10] G. D. Sprouse and L. A. Orozco, Annu. Rev. Nucl. Part. Sci. **47**, 429 (1997).
[11] *Proceedings of the NATO Advanced Study Institute on Trapped Particles and Fundamental Physics, Les Houches, France, 2000*, edited by S. N. Atutov *et al*. (Springer, NATO Science Series II, **51**).
[12] S. N. Atutov *et al*., Phys. Scr. **105**, 15 (2003); J. Opt. Soc. Am. B **20**, 953 (2003).
[13] W. Reisdorf, Z. Phys. A **300**, 277 (1981); W. Reisdorf and M. Schädel, Z. Phys. A **343**, 47 (1992).
[14] S. Beghini, C. Signorini, S. Lunardi, M. Morando, G. Fortuna, A. M. Stefanini, W. Meczynski, and R. Pengo, Nucl. Instrum. Methods Phys. Res. A **239**, 585 (1985).
[15] R. B. Firestone, in *Table of Isotopes*, edited by V. S. Shirly (Wiley, New York, 1996).
[16] K.-T. Brinkmann, A. L. Caraley, B. J. Fineman, N. Gan, J. Velkovska, and R. L. McGrath, Phys. Rev. C **50**, 309 (1994).
[17] R. N. Sagaidak and A. V. Yeremin, Nucl. Instrum. Methods Phys. Res. B **93**, 103 (1994).
[18] R. Bass, Phys. Rev. Lett. **39**, 265 (1977); Lect. Notes Phys. **117**, 281 (1980).
[19] W. Reisdorf *et al*., Nucl. Phys. **A438**, 212 (1985).
[20] C. H. Dasso, S. Landowne, and A. Winther, Nucl. Phys. **A407**, 221 (1983).
[21] S. Cohen, F. Plasil, and W. J. Swiatecki, Ann. Phys. (NY) **82**, 557 (1974).
[22] G. Audi and A. H. Wapstra, Nucl. Phys. **A595**, 509 (1995).
[23] M. Beckermann and M. Blann, Phys. Rev. C **17**, 1615 (1978); M. Blann and T. T. Komoto, Phys. Rev. C **26**, 472 (1982).
[24] A. N. Andreyev *et al*., Nucl. Phys. **A568**, 323 (1994); **A620**, 229 (1997); **A626**, 857 (1997).
[25] A. J. Sierk, Phys. Rev. C **33**, 2039 (1986).
[26] A. Yoshida *et al*., Phys. Lett. **B389**, 457 (1996).
[27] C. Signorini *et al*., Eur. Phys. J. A **2**, 227 (1998).
[28] T. Sikkeland, Phys. Rev. B **135**, 669 (1964).
[29] D. J. Hinde, R. J. Charity, G. S. Foote, J. R. Leigh, J. O. Newton, S. Ogaza, and A. Chatterjee, Nucl. Phys. **A452**, 550 (1986); D. J. Hinde (private communication).
[30] S. Baba *et al*., Z. Phys. A **331**, 53 (1988).
[31] R. N. Sagaidak *et al*., in *Proceedings of 10th International Conference on Nuclear Reaction Mechanisms, Varenna, Italy, 2003*, edited by E. Gadioli (Universitá degli Studi di Milano, Milan, 2003), p. 301; JINR Preprint E7-2003-149, Dubna, 2003.
[32] U. L. Businaro and S. Gallone, Nuovo Cimento **1**, 1277 (1955).